Effects of the spin-orbit interaction on the optical properties of ReS_2 and $ReSe_2$

Thorsten Deilmann *

Institut für Festkörpertheorie, Universität Münster, 48149 Münster, Germany

(Received 1 September 2023; revised 12 December 2023; accepted 13 December 2023; published 8 January 2024)

ReS_2 and $ReSe_2$ are less frequently studied transition metal dichalcogenides. They appear in the $1T'$ phase with a significantly reduced symmetry compared with, for example, MoS_2, while inversion symmetry is preserved. Several broad peaks have been observed in previous experimental measurements. The interpretation of their physical origin and properties is a challenging task without the help of theoretical insights. Here, we employ *ab initio* *GW*-Bethe-Salpeter equation calculations to investigate the optical properties of neutral and charged monolayers. We present a detailed analysis of the low-energy excitons and trions. In agreement with experiment, we find that the neutral excitons are strongly bound. In contrast, only a tiny trion binding energy of <10 meV is found. By artificially manipulating the spin-orbit coupling (SOC), we demonstrate its importance for the internal structure of the transitions. Interestingly, we find two optically active low-energy excitons. Both stem from transitions between the same valence and conduction bands. In the absence of SOC, only one peak (singlet) can be bright. Therefore, additional peaks are a direct manifestation of SOC on the optical properties.

DOI: 10.1103/PhysRevB.109.035111

I. INTRODUCTION

In recent years, transition metal dichalcogenides (TMDCs) have been a focus of interest [1]. Especially monolayers MX_2 (with M = Mo/W and X = S/Se/Te) has been investigated due to its interesting and promising optical properties [2,3] as well as many other exciting phenomena [4–6]. In these MX_2 materials, the physical origin of the optical response is vertical transitions at the $\pm K$ points of the Brillouin zone [7,8]. In the surroundings of these high-symmetry points, the spin-orbit interaction splits the valence and conduction bands, respectively, and leads to spin-layer locking [9,10] as well as spin-forbidden transitions [11–13]. Typically, two bright peaks are found (often labeled A and B), which stem from transitions between bands which are split by the spin-orbit coupling (SOC). Many further TMDCs have been found [14] or predicted [15], among them ReS_2 and $ReSe_2$ which are typically found in the distorted $1T$ (i.e., $1T'$) phase [16–21]. This means ReX_2 becomes asymmetric, and one-dimensional chains form [see Fig. 1(a)]. Nevertheless, these materials have inversion symmetry, and thus, all electronic states are twofold degenerated under the influence of SOC. At first glance, therefore, the effect of SOC appears to be less prominent than other MX_2 materials.

However, the quantum-mechanical details determine the light-matter interaction also in ReX_2. Because of the reduced dimension in the chainlike structure, the optical response of neutral and charged monolayer ReX_2 is dominated by energetic low-lying correlated many-body states, i.e., excitons and trions. Experimental measurements for ReS_2 by Wang *et al.* [22,23] have shown broad peaks with line widths of several tens of meV. By challenging fits, they concluded a large trion binding energy in monolayer ReS_2 with a size of $\sim$60 meV [22]. This surprisingly large value is about double the size of other Mo- or W-based TMDCs. In three-layer samples, the trion binding energy is still reported to be $\sim$20 meV [22,23]. On the other hand, in theoretical investigations, the quantum-mechanical states corresponding to these charged peaks are still missing, and thus, a physical explanation for such large trion binding energies is lacking. In Mo- or W-based TMDCs, several different phenomena, like dark states [11–13], phonon-assisted transitions [24,25], etc. [26], have emerged as additional peaks in the optical spectra. Similar phenomena are possible for ReX_2, and the identification of the quantum-mechanical origin solely based on photoluminescence (PL) measurements is challenging. Therefore, a detailed understanding of the low-energy optical spectrum of ReS_2 and $ReSe_2$ is still missing.

In this paper, we carry out first-principles calculations of the neutral and charged monolayers of ReX_2. We start by investigating the structural properties (Sec. II) and the electronic structure, focusing on the effects of spin-orbit interaction in Sec. III. By many-body perturbation theory, we find a realistic approximation of the electronic band gap in vacuum and above a substrate. To investigate the effect of the spin-orbit interaction in detail, we introduce an approach to vary its strength systematically. This methodology is generally applicable in *ab initio* calculations and especially important for the large class of two-dimensional (2D) materials including heavy elements [15]. In Sec. IV, we analyze the contributions to the optical response of neutral excitons and show how the spin-orbit interaction mixes the singlet and triplet states. As a consequence, more than one transition between the same bands becomes optically active which is a direct optical manifestation of the SOC. In the absence of SOC, only one bright peak (singlet) is possible, while the three triplet states are dark. Finally, we investigate the

*thorsten.deilmann@uni-muenster.de

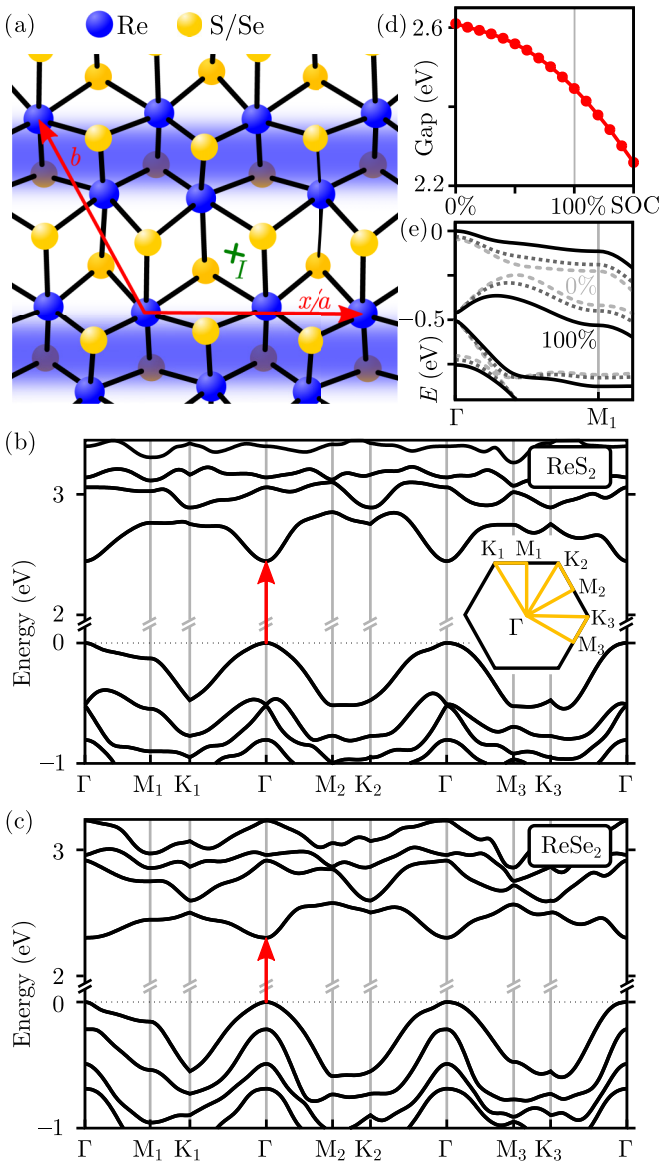

FIG. 1. (a) On-top view of the structure of ReX_2 (X = S/Se). The blue atoms denote rhenium, the yellow atoms sulfur/selenium. The lattice vectors of the unit cell are shown in red. Along the x direction (typically called a), quasi-one-dimensional stripes form, which are separated in the b direction. The blue stripes illustrate the quasi-one-dimensional character. An inversion center I is marked with a green cross. (b) GdW band structure of ReS_2. The path is shown in the Brillouin zone in the inset. The valence band maximum is set to zero energy. For optics, the transition close to Γ is the most important, which is denoted by the red arrow. (c) Same for $ReSe_2$. (d) Direct band gap in ReS_2 for different strength of the spin-orbit coupling (SOC) [see Eq. (2)]. (e) Zoom-in close to the valence band in ReS_2 for 0, 50, and 100% SOC.

charged monolayers in Sec. V, which should allow for a direct comparison with experiments [22,23]. In the limit of low doping, we find small trion binding energies of <10 meV, i.e., less than half compared with other monolayer MX_2 TMDCs. We compare theoretical and experimental results and discuss further possible interpretations of the measurements [22,23] in Sec. VI.

II. SYSTEM AND METHODS

ReS_2 and $ReSe_2$ consist of 2D layers. A top view of its structure is shown in Fig. 1(a). Like MX_2 TMDCs, the central layer consists of the transition metal, and a layer of S/Se is found above and below. In contrast to the 2H-like structure, the in-plane positions are shifted (1T prototype). The atoms in ReX_2 further relax to the so-called 1T' structure whose coordinates are shown. Its description requires a 2×2 cell, i.e., the unit cell consists of 12 atoms. The rhenium atoms relax closer to each other (with respect to the 1T prototype). In literature, this is commonly referred to as one-dimensional stripes [highlighted in blue in Fig. 1(a)]. However, they are connected by strong chemical bonds.

Our investigations of this system are based on *ab initio* methods. As a starting point, we perform a structural relaxation using density functional theory (DFT) [27,28]. On top of this, we evaluate the electronic structure including spin-orbit interaction [29–31]. Introducing spinors, the Kohn-Sham equations can be written in general [32] in the block structure:

$$\begin{bmatrix} H_0 + V_{\mathrm{xc}}^{11} + V_{\mathrm{SOC}}^{11} & V_{\mathrm{xc}}^{12} + V_{\mathrm{SOC}}^{12} \\ V_{\mathrm{xc}}^{21} + V_{\mathrm{SOC}}^{21} & H_0 + V_{\mathrm{xc}}^{22} + V_{\mathrm{SOC}}^{22} \end{bmatrix} \begin{pmatrix} \psi_{n,\mathbf{k}}^1 \\ \psi_{n,\mathbf{k}}^2 \end{pmatrix} = \epsilon_{n,\mathbf{k}} \begin{pmatrix} \psi_{n,\mathbf{k}}^1 \\ \psi_{n,\mathbf{k}}^2 \end{pmatrix}, \tag{1}$$

where $H_0 = -\Delta + V_{\mathrm{Coul}} + V_{\mathrm{ext}}$, and the spin-orbit interaction is fully included in V_{SOC}. In our calculations, we employ j-dependent pseudopotentials ($j = l \pm \frac{1}{2}$) [33,34]. We generate the pseudopotentials for atoms according to Hamann [35] including nonlinear core corrections [36]. For numerical efficiency, we employ the Kleinman-Bylander form [37,38]; V_{ext} denotes the local part of the pseudopotential. With V_{SOC}, we refer to the j-dependent scalar-relativistic and spin-orbit part [34]. If the SOC is (artificially) neglected, the remaining part is labeled $V_{\text{no-SOC}}$. We note in passing that we do not divide the scalar-relativistic and spin-orbit parts, which is possible in principle. For ReX_2, no spin polarization is present, and inversion symmetry simplifies the Hamiltonian: The off-diagonal parts are connected by complex conjugation, and the diagonal parts are equivalent. This results in twofold degenerated states. We underline that this can lead to arbitrary phases of the spinors, e.g., for the calculation of the electron-hole matrix elements (see below), where relative phases of infinitely small displaced $\mathbf{k}$ are important, we add an arbitrary small difference of $\pm\delta$ weighted by the overlap matrix (i.e., $H_0 \pm \delta S$, where δ is on the order of μeV to meV).

To investigate the importance of the SOC, we linearly mix the matrix elements:

$$V_{\mathrm{SOC}} \to \alpha V_{\mathrm{SOC}} + (1-\alpha) V_{\text{no-SOC}}. \tag{2}$$

For $\alpha = 1$, the SOC is fully included, while for $\alpha = 0$, the SOC is neglected. Mathematically, we can also simulate $\alpha > 1$, which would correspond to a hypothetical element with stronger SOC. ince V_{SOC} and $V_{\text{no-SOC}}$ are built by atomic pseudopotentials, the scaling of the SOC can be done for each atom individually. We note in passing that this approach corresponds to the well-known virtual crystal

approximation [39] which is frequently used for defects, for instance.

To gain a more reasonable approximation of the excited-state properties, we use many-body perturbation theory. In a first step, we use the *GW* approximation [40,41] to improve the electronic properties from DFT in Eq. (1), $\hat{\mathcal{H}}^{GW} = \hat{\mathcal{H}}^{\mathrm{DFT}} - V_{\mathrm{xc}} + iGW$. When evaluating self-energy $\Sigma = iGW$, all states of the same shell must be explicitly included in the calculation as valence states [42]. Therefore, we have used pseudopotentials with semicore states in contrast with our previous work [43]. After we have checked that the results are in reasonable agreement, we employ the more efficient *GdW* approximation [44,45]. By approximating $V_{\mathrm{xc}} \approx iGW_{\mathrm{metal}}$, we evaluate

$$\hat{\mathcal{H}}^{GdW} = \hat{\mathcal{H}}^{\mathrm{LDA}} + \overbrace{iG\underbrace{(W - W_{\mathrm{metal}})}_{dW}}^{\Delta\Sigma},$$

and the quasiparticle energies result in

$$E^{\mathrm{QP}}_{n\mathbf{k}} = E^{\mathrm{LDA}}_{n\mathbf{k}} + \langle n\mathbf{k}|\Delta\Sigma\big(E^{\mathrm{QP}}_{n\mathbf{k}}\big)|n\mathbf{k}\rangle.$$

For the calculation of the optical properties, the perturbation of one particle is not sufficient, and we have to evaluate the two-particle or (if doped) three-particle Hamiltonian. The Bethe-Salpeter equation [46,47] in the *GW*/*GdW* approximation leads to the Hamiltonian matrix elements:

$$\begin{aligned}\langle \mathbf{vc}|\hat{H}^{(eh)}|\mathbf{v'c'}\rangle = {} & \big(E^{\mathrm{QP}}_{\mathbf{c}} - E^{\mathrm{QP}}_{\mathbf{v}}\big)\delta_{\mathbf{cc'}}\delta_{\mathbf{vv'}} \\ & - (W_{\mathbf{v'c},\mathbf{vc'}} - V_{\mathbf{v'c},\mathbf{c'v}}).\end{aligned} \tag{3}$$

In addition to the energetic differences between the valence and conduction bands (on the diagonal), the screened direct interaction W (typically attractive) and the bare exchange interaction V (typically repulsive) enter. The strength of the SOC is adjusted by Eq. (2) and determines the corresponding spinors $\psi_{n,\mathbf{k}}$. By using these spinors in all steps of many-body perturbation theory, no further modifications for *GW*-BSE are required. For instance, in the case of the BSE Hamiltonian, the SOC implies that all elements are nonzero, and singlet and triplet states do not decouple [48]. In our *ab initio* extension for trions [49,50], we set up the three-particle Hamiltonian with the matrix elements:

$$\begin{aligned}&\langle \mathbf{vc}_1\mathbf{c}_2|\hat{H}^{(eeh)}|\mathbf{v'c}'_1\mathbf{c}'_2\rangle \\ &\quad = (\epsilon_{\mathbf{c}_1} + \epsilon_{\mathbf{c}_2} - \epsilon_{\mathbf{v}})\delta_{\mathbf{c}_1,\mathbf{c}'_1}\delta_{\mathbf{c}_2,\mathbf{c}'_2}\delta_{\mathbf{v},\mathbf{v'}} \\ &\qquad + \big(W_{\mathbf{c}_1\mathbf{c}_2,\mathbf{c}'_1\mathbf{c}'_2} - W_{\mathbf{c}_1\mathbf{c}_2,\mathbf{c}'_2\mathbf{c}'_1}\big)\delta_{\mathbf{v},\mathbf{v'}} \\ &\qquad - \big(W_{\mathbf{v'c}_1,\mathbf{vc}'_1} - V_{\mathbf{v'c}_1,\mathbf{c}'_1\mathbf{v}}\big)\delta_{\mathbf{c}_2,\mathbf{c}'_2} \\ &\qquad - \big(W_{\mathbf{v'c}_2,\mathbf{vc}'_2} - V_{\mathbf{v'c}_2,\mathbf{c}'_2\mathbf{v}}\big)\delta_{\mathbf{c}_1,\mathbf{c}'_1} \\ &\qquad + \big(W_{\mathbf{v'c}_1,\mathbf{vc}'_2} - V_{\mathbf{v'c}_1,\mathbf{c}'_2\mathbf{v}}\big)\delta_{\mathbf{c}_2,\mathbf{c}'_1} \\ &\qquad + \big(W_{\mathbf{v'c}_2,\mathbf{vc}'_1} - V_{\mathbf{v'c}_2,\mathbf{c}'_1\mathbf{v}}\big)\delta_{\mathbf{c}_1,\mathbf{c}'_2}.\end{aligned} \tag{4}$$

While the first line consists of the energetic differences, the second describes the (screened) interaction of both electrons, and the remaining terms the interaction of the hole with one of the electrons. Like the Bethe-Salpeter equation, we diagonalize $\hat{H}^{(eeh)}$, and the eigenvalues and eigenvectors lead to the trion energies and its wave functions [49]. Based on this, we can evaluate excitons and trions on the same footing, assuming the doping is sufficiently small.

III. ELECTRONIC PROPERTIES

Several aspects of the electronic properties of monolayer ReS_2 and $ReSe_2$ have previously been investigated in the literature in experimental and theoretical studies [16–22,51]. In this paper, we focus on the role of the SOC which will also become important for the calculation of the optical properties.

The band structures of ReX_2 are shown in Figs. 1(b) and 1(c). Both materials have a direct band gap at the Γ point. In *GdW*, we find values of 2.45 and 2.30 eV for ReS_2 and $ReSe_2$, respectively [43]. These values are in reasonable agreement with previous results [18,51]. Especially the valence bands of the two materials have clearly different dispersions, for instance, along $\Gamma-M_1$, $\Gamma-M_2$, and $\Gamma-M_3$. The results are shown with SOC fully included. If the SOC is not included, the overall structure of the bands remains similar (not shown). However, the band gap increases by ∼160 meV [for ReS_2 see Fig. 1(d)]. A more detailed view shows that the valence band is changing its dispersion, while the conduction band is rigidly shifted. Figure 1(e) shows a zoom-in along $\Gamma-M_1$ (where the largest changes are observed) from 0 to 100% SOC. While for 0% SOC, the topmost and second valence bands almost touch, a clear repulsion between these bands is observed if the SOC becomes stronger. Eventually, this results in a much flatter topmost valence band close to its maximum at Γ and the effective mass is reduced by ∼20%. A similar influence is obtained for $ReSe_2$ as well.

The differences of our many-body calculations with respect to the DFT result are the quasiparticle corrections. For ReS_2 and $ReSe_2$, these quasiparticle corrections are large and have similar sizes of 1.1 eV. In 2D materials, appreciable values are common due to the reduced screening [15]; in ReX_2, they are at the upper limit. On the other hand, this makes the band gap highly tunable by the surrounding of the monolayer (e.g., the substrate). To estimate the size of this effect, we approximate a substrate by its dielectric screening; for details, see our previous studies [50,52]. This leads to a reduction of the band gap by ∼0.3 eV, if the dielectric screening of the substrate is like that of bulk ReX_2. Contrariwise, the optical properties discussed in the next Secs. IV and V are hardly changed by a substrate [50]. For the converged result in Fig. 1, we employ an 8×8 mesh to evaluate the integral for Σ. A denser mesh of 16×16 points is required to calculate the dielectric function. For *GdW*, the three-center integrals employ an auxiliary basis of 627 plane waves (2 Ry), while for the comparison to *GW*, we use 1420 Gaussian functions and 101 plane waves.

IV. OPTICAL PROPERTIES: EXCITONS

Authors of previous studies [18,51] on the absorption of monolayer ReX_2 have shown a multitude of peaks at energies below the electronic band gap. To get further insights into their origin, we employ the Bethe-Salpeter equation [46,47], whose solution leads to exciton energies Ω^S and the corresponding wave functions $|S\rangle = \sum_{v,c} B^S_{v,c}|vc\rangle$. By employing Eq. (2), we systematically change the strength of the SOC seen by the excitons [53]. The upper panel of Fig. 2(a) shows the peak

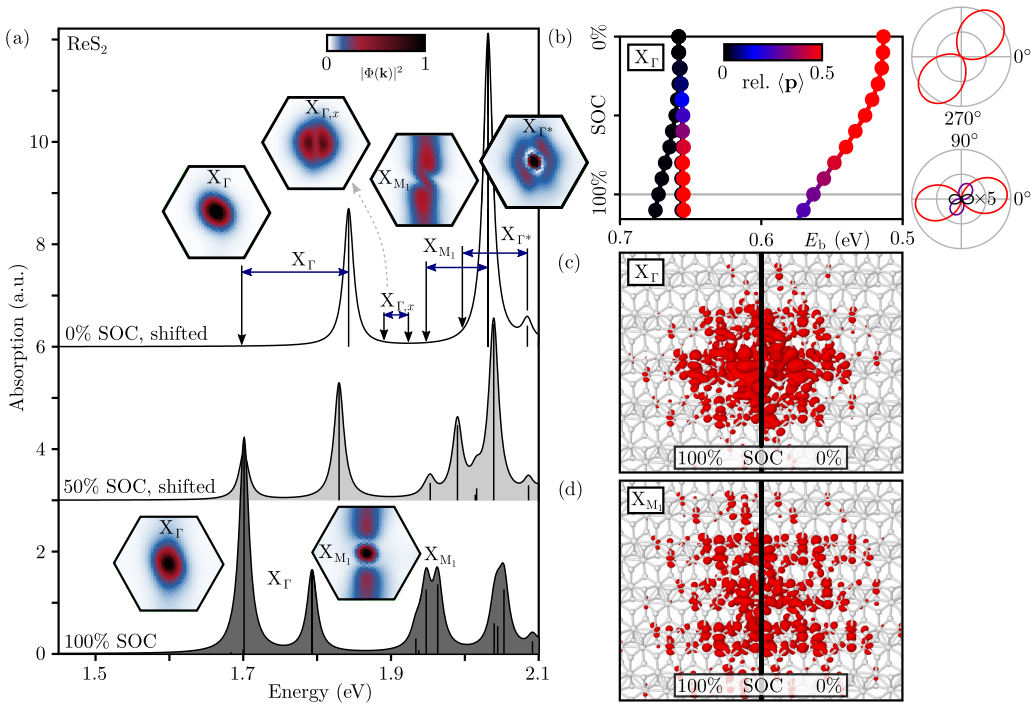

FIG. 2. (a) Absorption of monolayer ReS_2 depending on the spin-orbit coupling (SOC). 0, 50, and 100% SOC are vertically shifted for clarity. An artificial broadening of 8 meV is used. The vertical arrows indicate the positions of dark peaks, the horizontal (dark blue) arrows show the corresponding singlet-triplet splittings. Furthermore, 0 and 50% are horizontally shifted by the changes of the band gap shown in Fig. 1(d). Close to the corresponding peaks the extension in **k** space is shown for the first excitations X_Γ, X_{M_1} as well as $X_{\Gamma,x}$ and X_{Γ^*}. (b) Analysis of the binding energy [difference of gap in Fig. 1(d) and exciton peak in (a)] and relative oscillator strength of the first four X_Γ transitions with respect to the SOC. The right panel shows the polarization dependent oscillator strength for 0 and 100%, respectively. The colors from the left panel are used, and the strength of the two lowest states (black) is increased by a factor of 5. (c) and (d) Comparison of the real-space visualization of X_Γ and X_{M_1} (left panel 100% SOC, right 0% SOC). The holes are centered in the middle close to a rhenium atom, respectively.

structure of bright singlet excitations and the corresponding three (degenerated) triplets lower in energy (vertical arrows). The horizontal arrows mark the singlet-triplet splitting of each exciton and are clearly different for the different excitons. The exciton around Γ has the lowest energy and is denoted as X_Γ with energies of 1.70 (triplet) and 1.84 eV (singlet), respectively. Note that the upper panels are shifted by the change of the band structure gap, as shown in Fig. 1(d). The corresponding exciton amplitude in the first Brillouin zone is shown above with the highest intensities marked in red-black. This inset confirms the assignment and also clarifies the slightly asymmetric shape around Γ of the adsorption shown in the lowest panel of Fig. 2(a). The next peaks belong to $X_{\Gamma,x}$ and are all dark; the reciprocal space shows a node line crossing Γ. We note in passing that its singlet-triplet splitting is much smaller, only 30 meV. Furthermore, the next two bright peaks X_{M_1} and X_{Γ^*} and their corresponding triplet states are labeled. While X_{M_1} is oriented in the M_1 direction, X_{Γ^*} appears to be an excited state with a nodal ring around the maximum at Γ.

Increasing the SOC to 100% allows us to follow the shift of the peaks as well as the mixing of singlet and triplet states. For X_Γ, we find that two bright states finally move to 1.70 and 1.79 eV; the first dark state is at 1.68 eV. Figure 2(b) focuses on this exciton and shows many more mixtures. Due to the SOC-mediated mixing, the four peaks become energetically closer, and the amplitude is transferred. If the SOC is negligible, the states are built up by $\Psi_{\downarrow\uparrow}$, $\Psi_{\uparrow\downarrow}$, and $[\Psi_{\uparrow\uparrow} + \Psi_{\downarrow\downarrow}]/\sqrt{2}$ for triplet states and $[\Psi_{\uparrow\uparrow} - \Psi_{\downarrow\downarrow}]/\sqrt{2}$ for the singlet state (the first spin (of the hole) is reversed compared with the electron, see Ref. [46]). Increasing the SOC enhances the coupling between the last two states (if SOC is fully included, >90% remains from these configurations). The detailed structure of the excitonic wave functions of X_Γ is slightly rotated, which is the result of the changed valence bands discussed in Fig. 1(e). Here, X_{M_1} alters its character even more drastically when varying the SOC. It can be regarded as a mixture of the previous X_{M_1} and X_{Γ^*} without SOC. The amplitude shows a clear maximum at Γ, a nodal ring, and further contributions in the M_1 direction.

In addition to the exciton wave function in reciprocal space $\Phi(\mathbf{k})$, we also show the real-space wave function of X_Γ and X_{M_1} with and without SOC in Figs. 2(c) and 2(d). The hole is centered in the middle of the image close to a rhenium atom, and the left/right panels show 100%/0% SOC, respectively. Both reciprocal and real-space wave functions are point symmetric and can thus be compared directly. In sum, the real-space properties seem to be much more robust against changes of the SOC than the reciprocal-space images discussed before. However, a detailed comparison of X_{M_1} shows a slightly different shape, i.e., due to SOC, the exciton is slightly more extended in the y direction. The mixture of excitons is an important property and is experimentally accessible indirectly

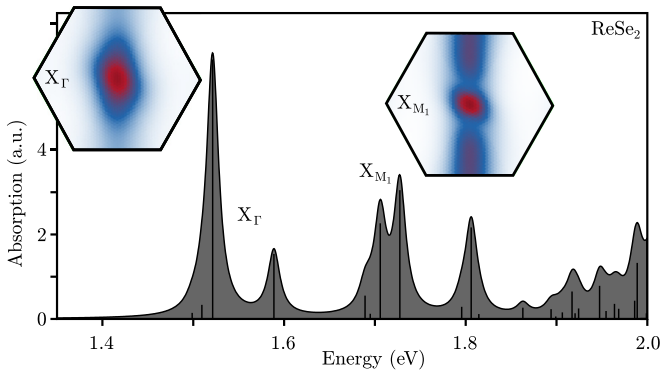

FIG. 3. Optical absorption of monolayer $ReSe_2$. Spin-orbit coupling (SOC) is fully included, i.e., compare with Fig. 2(a), lower panel. For further details, see the caption of Fig. 2.

by the response to magnetic fields [54]. For instance, for intra- and interlayer transitions [55], similar mixtures of excitons have been observed. We note in passing that adding $\pm\delta$ in Eq. (1) is essential to ensure the correct evaluation of the electron-hole interaction and the exciton wave function (see discussion above). For $ReSe_2$ (see Fig. 3), the overall situation is like ReS_2. Due to the smaller electronic band gap, the optical gap is also lower in energy. Again, we find several peaks; most of them can be assigned to small groups. The first X_Γ exciton can be found at 1.50 eV; two of the four mixed peaks carry the main optical weight. The contribution is mostly localized around Γ, and the distribution is quite similar to that of ReS_2. Also, the second-lowest peak X_{M_1} makes no exception and is similarly mixed from contributions to M_1 and an excited state (calculation without SOC not shown for $ReSe_2$). Compared with ReS_2, several details vary, i.e., the peak splittings are a bit smaller, and their relative weights vary. In sum, both materials have a very similar optical response for the neutral monolayers. Because this is true for doped materials as well, we mostly concentrate on ReS_2 in the next section.

V. OPTICAL PROPERTIES OF CHARGED MONOLAYERS

Now we move to the situation in which the semiconducting monolayers are doped. The source of the additional charges is not important; they may stem from defects [56], applied electric fields [57], or similar. For a description from first principles, we employ Eq. (4) discussed in the Methods Sec. II. To compare with the mentioned available experimental measurements, we focus on ReS_2 and negatively charged doping in Fig. 4. For $ReSe_2$, we find qualitatively similar results (not discussed here). The upper/lower panels of Fig. 4 show the optical absorption of ReS_2 without/with SOC. The corresponding black curve is the weight due to the excitons already discussed in Fig. 2. The green curves show the influence of the doping. Neglecting SOC, the first bright trion and exciton are found at nearly the same energy. For the lowest dark transitions (marked by the arrows), the trion binding energy is just above 10 meV. At higher energies, we find several further states (above ∼1.9 eV, the Haydock recursion scheme [58] is used because it requires less computational effort). However, their exact position and oscillator strength are not

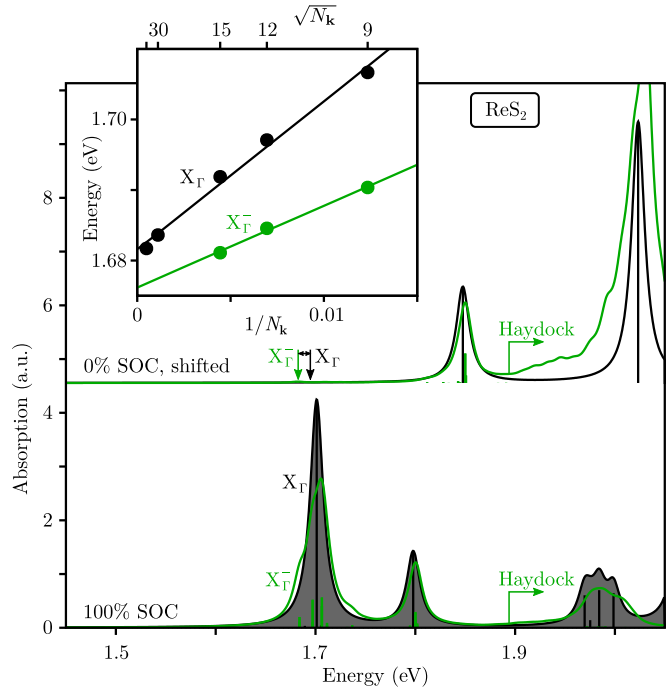

FIG. 4. Optical absorption of ReS_2 in negatively charged monolayers. The upper panel shows the results without spin-orbit coupling (SOC), the arrows mark the lowest dark transitions. The lower panel shows the spectrum if SOC is fully included. These green curves are compared with the corresponding neutral exciton spectrum (black, 15×15 mesh, like in Fig. 2). Above ∼1.9 eV, the spectrum is evaluated using the Haydock recursion scheme. The inset shows the energies for different N_k, where the extrapolation $1/N_\mathbf{k} \to 0$ determines the trion binding energy.

fully converged with the employed 15×15 mesh at such high energies. If we turn on the artificially neglected SOC, we find the absorption shown in the lower panel of Fig. 4. In addition to the two strong absorption peaks of the excitons, the lowest (bright) trion shows up as a shoulder in our calculation (with the chosen artificial Lorentzian broadening of 8 meV). The difference of the first bright peaks is the trion binding energy and can be measured in experiment. In the limit of vanishing doping, our calculated binding energy is ∼10 meV (inset in Fig. 4 extrapolated to zero). This value is much smaller than our calculations for other TMDCs (∼40 meV [50]).

Furthermore, we have calculated the properties of positively charged states (not shown). Compared with the negative doping discussed above, we find an almost identical trion binding energy. Therefore, we conclude that trionic effects are small in ReX_2.

VI. COMPARISON WITH EXPERIMENT

In the literature, there are several studies on the optical properties, which we will briefly summarize here. For monolayer ReS_2, Tongay *et al.* [16] found one broad peak at ∼1.6 eV. Jadczak *et al.* [19] were able to resolve a substructure of two peaks at ∼1.66 and 1.72 eV. With their measurements, Wang *et al.* [22,23] also showed two main peaks at ∼1.66 and 1.73 eV and found three more peaks by fitting

the shoulders. Two of these were attributed to trions corresponding to the two main excitons, and a trion binding energy of ∼60 meV was inferred. Similar studies have been carried out for 2–5 layers, and a very moderate change in intensities with carrier density as well as polarization dependence was observed for the 3*L* sample [22,23]. In the optical properties of $ReSe_2$, two peaks are found at 1.50 and 1.55 eV [51].

In our calculations of the optical properties for neutral systems, we find peaks at 1.70 and 1.79 eV for ReS_2 and 1.52 and 1.59 eV for $ReSe_2$. Both results are in good agreement with experimental data down to differences of <50 meV. This is also true for the polarization dependence [Fig. 2(b)] for the monolayer compared with 3*L* [22]). When we simulate the doped system, we find that the first excitation is <10 meV lower with respect to the corresponding exciton. Although we do not simulate all the effects that occur at higher doping (e.g., band renormalization and additional screening), we can estimate the changes for higher doping concentrations [59]. The inset in Fig. 4 shows only a moderate increase of the trion binding energy. Therefore, we do not expect a large increase for moderate doping (i.e., fewer $N_{\mathbf{k}}$). Experimentally, trions have only been detected in the works of Wang *et al.* [22,23], while they are absent in the other samples/measurements reported in the literature. We note that, in their results (extrapolated to zero doping), the first peak associated with trions does not disappear (only its intensity decreases), and the associated trion binding energies of the first and the second state are different. From our calculations, we find that the first two excitons are transitions between the same bands, suggesting similar energetics. In summary, our calculations do not support the interpretation that trions with strong binding energies are present in ReX_2. We can only speculate about other reasons, e.g., the PL measurements might lead to intensities for states interacting with phonons [26], or the dielectric screening may vary across the sample [50].

VII. CONCLUSIONS

We studied the electronic and optical properties of ReS_2 and $ReSe_2$. Varying the spin-orbit interaction allows us to understand the origin of the possible low-energy excitations. The neutral excitons have strong binding energies up to 0.8 eV and can be found in multipeak structures. The spin-orbit interaction has mixed singlet and triplet states as well as their optical amplitudes. Two peaks share the optical absorption. Furthermore, also excitons with different character have hybridized. When the system becomes doped, the absorption changes only slightly. In the limit of low doping, we calculate a trion binding energy of <10 meV. We conclude that this does not support the previous experimental interpretation of strongly bound trions but may point to other origins of the experimentally observed peaks.

ACKNOWLEDGMENTS

The authors thank Peter Krüger and Ashish Arora for fruitful discussions. The authors acknowledge financial support from the Deutsche Forschungsgemeinschaft through Project No. 426726249 (DE 2749/2-1 and DE 2749/2-2). The authors gratefully acknowledge the Gauss Centre for Supercomputing e.V. [60] for funding this project by providing computing time through the John von Neumann Institute for Computing on the GCS Supercomputer JUWELS [61] at Jülich Supercomputing Centre.

[1] G. Wang, A. Chernikov, M. M. Glazov, T. F. Heinz, X. Marie, T. Amand, and B. Urbaszek, Excitons in atomically thin transition metal dichalcogenides, Rev. Mod. Phys. **90**, 021001 (2018).

[2] K. F. Mak, C. Lee, J. Hone, J. Shan, and T. F. Heinz, Atomically thin MoS_2: A new direct-gap semiconductor, Phys. Rev. Lett. **105**, 136805 (2010).

[3] K. F. Mak, K. He, C. Lee, G. H. Lee, J. Hone, T. F. Heinz, and J. Shan, Tightly bound trions in monolayer MoS_2, Nat. Mater. **12**, 207 (2013).

[4] J. A. Wilson and A. D. Yoffe, The transition metal dichalcogenides discussion and interpretation of the observed optical, electrical and structural properties, Adv. Phys. **18**, 193 (1969).

[5] J. P. Eisenstein and A. H. MacDonald, Bose-einstein condensation of excitons in bilayer electron systems, Nature (London) **432**, 691 (2004).

[6] Y.-M. Li, J. Li, L.-K. Shi, D. Zhang, W. Yang, and K. Chang, Light-induced exciton spin Hall effect in van der Waals Heterostructures, Phys. Rev. Lett. **115**, 166804 (2015).

[7] D. Y. Qiu, F. H. da Jornada, and S. G. Louie, Optical spectrum of MoS_2: Many-body effects and diversity of exciton states, Phys. Rev. Lett. **111**, 216805 (2013).

[8] A. Ramasubramaniam, D. Naveh, and E. Towe, Tunable band gaps in bilayer transition-metal dichalcogenides, Phys. Rev. B **84**, 205325 (2011).

[9] Z. Gong, G.-B. Liu, H. Yu, D. Xiao, X. Cui, X. Xu, and W. Yao, Magnetoelectric effects and valley-controlled spin quantum gates in transition metal dichalcogenide bilayers, Nat. Commun. **4**, 2053 (2013).

[10] A. M. Jones, H. Yu, J. S. Ross, P. Klement, N. J. Ghimire, J. Yan, D. G. Mandrus, W. Yao, and X. Xu, Spin-layer locking effects in optical orientation of exciton spin in bilayer WSe_2, Nat. Phys. **10**, 130 (2014).

[11] C. Robert, T. Amand, F. Cadiz, D. Lagarde, E. Courtade, M. Manca, T. Taniguchi, K. Watanabe, B. Urbaszek, and X. Marie, Fine structure and lifetime of dark excitons in transition metal dichalcogenide monolayers, Phys. Rev. B **96**, 155423 (2017).

[12] T. Deilmann and K. S. Thygesen, Dark excitations in monolayer transition metal dichalcogenides, Phys. Rev. B **96**, 201113(R) (2017).

[13] A. Arora, N. K. Wessling, T. Deilmann, T. Reichenauer, P. Steeger, P. Kossacki, M. Potemski, S. Michaelis de Vasconcellos, M. Rohlfing, and R. Bratschitsch, Dark trions govern the temperature-dependent optical absorption and emission of doped atomically thin semiconductors, Phys. Rev. B **101**, 241413(R) (2020).

[14] H.-J. Lamfers, A. Meetsma, G. A. Wiegers, and J. L. de Boer, The crystal structure of some rhenium and technetium dichalcogenides, J. Alloys Compd. **241**, 34 (1996).

[15] S. Haastrup, M. Strange, M. Pandey, T. Deilmann, P. S. Schmidt, N. F. Hinsche, M. N. Gjerding, D. Torelli, P. M. Larsen, A. C. Riis-Jensen *et al.*, The computational 2D materials database: High-throughput modeling and discovery of atomically thin crystals, 2D Mater. **5**, 042002 (2018).

[16] S. Tongay, H. Sahin, C. Ko, A. Luce, W. Fan, K. Liu, J. Zhou, Y.-S. Huang, C.-H. Ho, J. Yan *et al.*, Monolayer behaviour in bulk ReS_2 due to electronic and vibrational decoupling, Nat. Commun. **5**, 3252 (2014).

[17] H. Wang, E. Liu, Y. Wang, B. Wan, C.-H. Ho, F. Miao, and X. G. Wan, Cleavage tendency of anisotropic two-dimensional materials: ReX_2 (X = S,Se) and WTe_2, Phys. Rev. B **96**, 165418 (2017).

[18] J. P. Echeverry and I. C. Gerber, Theoretical investigations of the anisotropic optical properties of distorted 1*T*ReS_2 and $ReSe_2$ monolayers, bilayers, and in the bulk limit, Phys. Rev. B **97**, 075123 (2018).

[19] J. Jadczak, J. Kutrowska-Girzycka, T. Smoleński, P. Kossacki, Y. S. Huang, and L. Bryja, Exciton binding energy and hydrogenic rydberg series in layered ReS_2, Sci. Rep. **9**, 1578 (2019).

[20] R. Oliva, M. Laurien, F. Dybala, J. Kopaczek, Y. Qin, S. Tongay, O. Rubel, and R. Kudrawiec, Pressure dependence of direct optical transitions in ReS_2 and $ReSe_2$, npj 2D Mater. Appl. **3**, 20 (2019).

[21] A. Dhara, D. Chakrabarty, P. Das, A. K. Pattanayak, S. Paul, S. Mukherjee, and S. Dhara, Additional excitonic features and momentum-dark states in ReS_2, Phys. Rev. B **102**, 161404(R) (2020).

[22] X. Wang, K. Shinokita, Y. Miyauchi, N. T. Cuong, S. Okada, and K. Matsuda, Experimental evidence of anisotropic and stable charged excitons (trions) in atomically thin 2D ReS_2, Adv. Funct. Mater. **29**, 1905961 (2019).

[23] X. Wang, K. Shinokita, and K. Matsuda, Radiative lifetime and dynamics of trions in few-layered ReS_2, Appl. Phys. Lett. **119**, 113103 (2021).

[24] D. Christiansen, M. Selig, G. Berghäuser, R. Schmidt, I. Niehues, R. Schneider, A. Arora, S. M. de Vasconcellos, R. Bratschitsch, E. Malic *et al.*, Phonon sidebands in monolayer transition metal dichalcogenides, Phys. Rev. Lett. **119**, 187402 (2017).

[25] E. Liu, J. van Baren, T. Taniguchi, K. Watanabe, Y.-C. Chang, and C. H. Lui, Valley-selective chiral phonon replicas of dark excitons and trions in monolayer WSe_2, Phys. Rev. Res. **1**, 032007(R) (2019).

[26] M. Yang, L. Ren, C. Robert, D. V. Tuan, L. Lombez, B. Urbaszek, X. Marie, and H. Dery, Relaxation and darkening of excitonic complexes in electrostatically doped monolayer WSe_2: Roles of exciton-electron and trion-electron interactions, Phys. Rev. B **105**, 085302 (2022).

[27] W. Kohn and L. J. Sham, Self-consistent equations including exchange and correlation effects, Phys. Rev. **140**, A1133 (1965).

[28] T. Deilmann, P. Krüger, M. Rohlfing, and D. Wegner, Adsorption and STM imaging of tetracyanoethylene on Ag(001): An *ab initio* study, Phys. Rev. B **89**, 045405 (2014).

[29] R. M. Dreizler and E. K. U. Gross, *Density Functional Theory* (Springer, Berlin, 1990).

[30] L. M. Sandratskii, Noncollinear magnetism in itinerant-electron systems: Theory and applications, Adv. Phys. **47**, 91 (1998).

[31] B. Stärk, P. Krüger, and J. Pollmann, Magnetic anisotropy of thin Co and Ni films on diamond surfaces, Phys. Rev. B **84**, 195316 (2011).

[32] T. Deilmann, Valley selectivity induced by magnetic adsorbates: Triplet oxygen on monolayer MoS_2, Phys. Rev. B **101**, 085130 (2020).

[33] G. B. Bachelet, D. R. Hamann, and M. Schlüter, Pseudopotentials that work: From H to Pu, Phys. Rev. B **26**, 4199 (1982).

[34] L. A. Hemstreet, C. Y. Fong, and J. S. Nelson, First-principles calculations of spin-orbit splittings in solids using nonlocal separable pseudopotentials, Phys. Rev. B **47**, 4238 (1993).

[35] D. R. Hamann, Generalized norm-conserving pseudopotentials, Phys. Rev. B **40**, 2980 (1989).

[36] S. G. Louie, S. Froyen, and M. L. Cohen, Nonlinear ionic pseudopotentials in spin-density-functional calculations, Phys. Rev. B **26**, 1738 (1982).

[37] L. Kleinman and D. M. Bylander, Efficacious form for model pseudopotentials, Phys. Rev. Lett. **48**, 1425 (1982).

[38] M. J. T. Oliveira and F. Nogueira, Generating relativistic pseudo-potentials with explicit incorporation of semi-core states using APE, the atomic pseudo-potentials engine, Comput. Phys. Commun. **178**, 524 (2008).

[39] L. Bellaiche and D. Vanderbilt, Virtual crystal approximation revisited: Application to dielectric and piezoelectric properties of perovskites, Phys. Rev. B **61**, 7877 (2000).

[40] L. Hedin, New method for calculating the one-particle green's function with application to the electron-gas problem, Phys. Rev. **139**, A796 (1965).

[41] M. Rohlfing, P. Krüger, and J. Pollmann, Quasiparticle band-structure calculations for C, Si, Ge, GaAs, and SiC using Gaussian-orbital basis sets, Phys. Rev. B **48**, 17791 (1993).

[42] M. Rohlfing, P. Krüger, and J. Pollmann, Quasiparticle band structure of CdS, Phys. Rev. Lett. **75**, 3489 (1995).

[43] Note that, in comparison with our previous study of $ReSe_2$ [51], we employ a semicore pseudopotential for rhenium, i.e., 14 electrons are described explicitly. The explains the small differences of 140 meV.

[44] M. Rohlfing, Electronic excitations from a perturbative LDA+GdW approach, Phys. Rev. B **82**, 205127 (2010).

[45] M. Drüppel, T. Deilmann, J. Noky, P. Marauhn, P. Krüger, and M. Rohlfing, Electronic excitations in transition metal dichalcogenide monolayers from an LDA+*GdW* approach, Phys. Rev. B **98**, 155433 (2018).

[46] M. Rohlfing and S. G. Louie, Electron-hole excitations and optical spectra from first principles, Phys. Rev. B **62**, 4927 (2000).

[47] G. Onida, L. Reining, and A. Rubio, Electronic excitations: Density-functional versus many-body Green's-function approaches, Rev. Mod. Phys. **74**, 601 (2002).

[48] M. Marsili, A. Molina-Sánchez, M. Palummo, D. Sangalli, and A. Marini, Spinorial formulation of the *GW*-BSE equations and spin properties of excitons in two-dimensional transition metal dichalcogenides, Phys. Rev. B **103**, 155152 (2021).

[49] T. Deilmann, M. Drüppel, and M. Rohlfing, Three-particle correlation from a many-body perspective: Trions in a carbon nanotube, Phys. Rev. Lett. **116**, 196804 (2016).

[50] M. Drüppel, T. Deilmann, P. Krüger, and M. Rohlfing, Diversity of trion states and substrate effects in the optical properties of an MoS_2 monolayer, Nat. Commun. **8**, 2117 (2017).

[51] A. Arora, J. Noky, M. Drüppel, B. Jariwala, T. Deilmann, R. Schneider, R. Schmidt, O. Del Pozo-Zamudio, T. Stiehm, A. Bhattacharya *et al.*, Highly anisotropic in-plane excitons in atomically thin and bulklike $1T'$-$ReSe_2$, Nano Lett. **17**, 3202 (2017).

[52] T. Esat, T. Deilmann, B. Lechtenberg, C. Wagner, P. Krüger, R. Temirov, F. B. Anders, M. Rohlfing, and F. S. Tautz, Transfering spin into an extended π orbital of a large molecule, Phys. Rev. B **91**, 144415 (2015).

[53] For the BSE and the calculations of trions, we employ at least a 15×15 mesh. Eight valence and eight conduction bands are considered; due to the inversion symmetry, each pair of bands forms a degenerate pair. Thus, the excitons are converged better than 10 meV.

[54] A. Arora, Magneto-optics of layered two-dimensional semiconductors and heterostructures: Progress and prospects, J. Appl. Phys. **129**, 120902 (2021).

[55] M.-C. Heißenbüttel, P. Marauhn, T. Deilmann, P. Krüger, and M. Rohlfing, Nature of the excited states of layered systems and molecular excimers: Exciplex states and their dependence on structure, Phys. Rev. B **99**, 035425 (2019).

[56] P. K. Gogoi, Z. Hu, Q. Wang, A. Carvalho, D. Schmidt, X. Yin, Y. H. Chang, L. J. Li, C. H. Sow, A. H. C. Neto *et al.*, Oxygen passivation mediated tunability of trion and excitons in MoS_2, Phys. Rev. Lett. **119**, 077402 (2017).

[57] E. Liu, J. van Baren, Z. Lu, M. M. Altaiary, T. Taniguchi, K. Watanabe, D. Smirnov, and C. H. Lui, Gate tunable dark trions in monolayer WSe_2, Phys. Rev. Lett. **123**, 027401 (2019).

[58] R. Haydock, V. Heine, and M. J. Kelly, Electronic structure based on the local atomic environment for tight-binding bands, J. Phys. C **5**, 2845 (1972).

[59] R. Tempelaar and T. C. Berkelbach, Many-body simulation of two-dimensional electronic spectroscopy of excitons and trions in monolayer transition metal dichalcogenides, Nat. Commun. **10**, 3419 (2019).

[60] www.gauss-centre.eu.

[61] D. Alvarez, JUWELS Cluster and Booster: Exascale Pathfinder with Modular Supercomputing Architecture at Juelich Supercomputing Centre, J. Large-Scale Res. Facilities **7**, A138 (2021).